SCIENTIFIC REPORTS

OPEN

New Insulating Antiferromagnetic Quaternary Iridates MLa$_{10}$Ir$_4$O$_{24}$ (M = Sr, Ba)

Received: 28 October 2014
Accepted: 27 May 2015
Published: 01 July 2015

Qingbiao Zhao[1,*], Fei Han[1], Constantinos C. Stoumpos[1], Tian-Heng Han[1,2], Hao Li[1] & J. F. Mitchell[1]

Recently, oxides of Ir^{4+} have received renewed attention in the condensed matter physics community, as it has been reported that certain iridates have a strongly spin-orbital coupled (SOC) electronic state, J_{eff} = ½, that defines the electronic and magnetic properties. The canonical example is the Ruddlesden-Popper compound Sr_2IrO_4, which has been suggested as a potential route to a new class of high temperature superconductor due to the formal analogy between J_{eff} = ½ and the S = ½ state of the cuprate superconductors. The quest for other iridium oxides that present tests of the underlying SOC physics is underway. In this spirit, here we report the synthesis and physical properties of two new quaternary tetravalent iridates, MLa$_{10}$Ir$_4$O$_{24}$ (M = Sr, Ba). The crystal structure of both compounds features isolated IrO_6 octahedra in which the electronic configuration of Ir is d^5. Both compounds order antiferromagnetically despite the lack of obvious superexchange pathways, and resistivity measurement shows that SrLa$_{10}$Ir$_4$O$_{24}$ is an insulator.

Electrons in 3*d* transition metal oxides exhibit correlated behavior because the bandwidth, W, is relatively narrow, while the electron-electron repulsion, parametrized by a Hubbard U, is significant. The result is a set of collective phenomena including high temperature superconductivity[1] and colossal magnetoresistance[2,3]. On the other hand, 5*d* transition metals are characterized by more extended orbitals, and in general, are expected to be uncorrelated metals, as for example IrO_2[4] and $Bi_2Ir_2O_7$[5]. Recently, however, Kim *et al.* found that strong spin-orbital coupling in the layered compound Sr_2IrO_4 leads to a relatively narrow J_{eff} = ½ band whose width is of the same scale as electron correlation, yielding a Mott insulating state[6,7]. With a square IrO_2 network, a $U/W \sim 1$, and a magnon dispersion qualitatively the same as cuprates[8], Sr_2IrO_4 has been studied intensely as a potential route to a new class of high temperature superconductor[8–10]. Some known iridates, including Ba_2IrO_4[11] and Ca_4IrO_6[12], have already shown behavior consistent with a J_{eff} = ½ description by resonant inelastic X-ray scattering, indicating that the phase space of J_{eff} = ½ materials extends beyond Sr_2IrO_4. These discoveries underscore the importance of identifying new iridates with J_{eff} = ½ states to better understand the phenomenology of these unusual correlated oxides.

The scope of the present work lies firmly in the regime of discovery synthesis of new compounds in a relatively unexplored regime of crystal chemistry as a first step on the way to classifying and understanding the breadth of spin-orbit driven physics in iridates. Toward this end, we have synthesized two new isostructural tetravalent iridates, MLa$_{10}$Ir$_4$O$_{24}$ (M = Sr, Ba) and characterized their crystal structures and magnetic, transport, and thermodynamic signatures. Each is comprised of isolated IrO_6 octahedra in which the nominal electronic configuration of Ir is d^5. They both order antiferromagnetically, and resistivity measurement shows that SrLa$_{10}$Ir$_4$O$_{24}$ exhibits insulating behavior.

[1]Materials Science Division, Argonne National Laboratory, Argonne, Illinois 60439, United States. [2]Department of Physics, University of Chicago, Chicago, IL 60637, USA. *Current address: Shanghai Institute of Ceramics, Chinese Academy of Sciences, Shanghai, 200033, China. Correspondence and requests for materials should be addressed to Q.Z. (email: qbzustc@gmail.com)

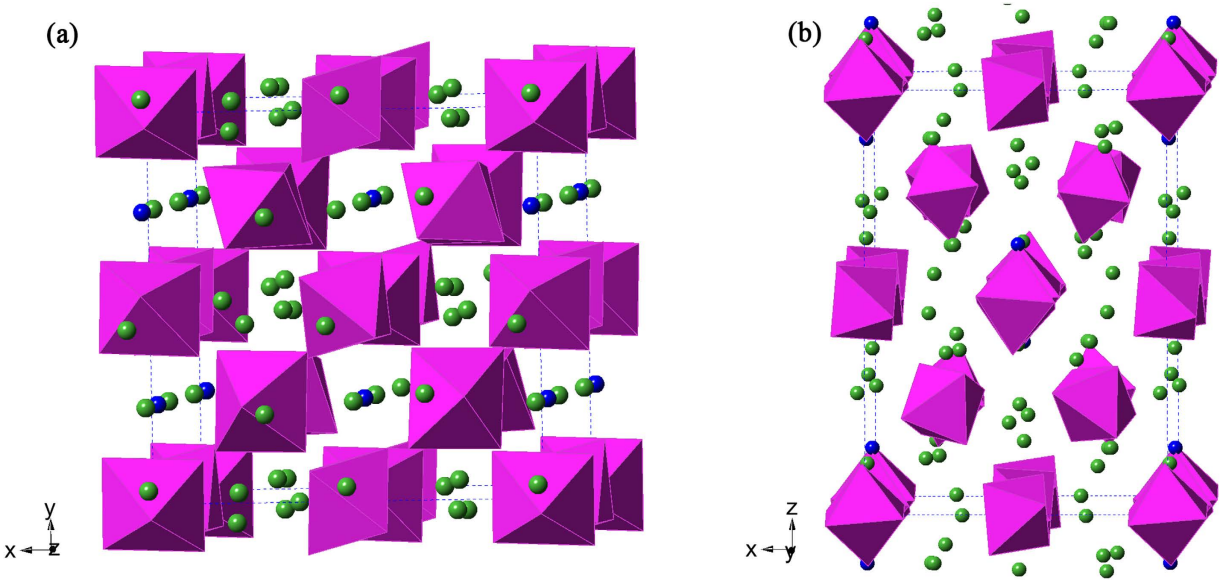

Figure 1. The crystal structure of MLa$_{10}$Ir$_4$O$_{24}$ (M = Sr, Ba). The purple color denotes IrO$_6$ octahedra, and the green and blue spheres denote La and M atoms (M = Sr, Ba), respectively (**a**) viewed from approximately (001) direction (**b**) viewed approximately from (010) direction.

The extensively studied iridates are mostly ternary oxides, which is likely due to the lack of approaches for crystallizing iridates that are compositionally diverse. To expand the horizon in studying iridates as J_{eff} = 1/2 candidates, quaternary and even higher order iridates are desired. Here it is demonstrated that high order iridates can be made with a facile flux crystal growth approach.

Results

Lattice constants and space group ($I4_1/a$) extracted from single-crystal diffraction measurements were similar to that of the known compound $Sr_9La_2Mo_4O_{24}$[13], and indeed the crystal structures (see Fig. 1) of the iridates could be solved from this starting model. For $SrLa_{10}Ir_4O_{24}$, no discernible site mixing between Sr and La was found in the refinement. For $BaLa_{10}Ir_4O_{24}$, the Ba and La sites were assigned based on the apparent differences in bond lengths of Ba-O and La-O. The structure features isolated IrO$_6$ octahedra with M (M = Sr, Ba) and La atoms located interstitially. There are two independent Ir sites, both occupying special positions, with the Ir atoms in a distorted octahedral coordination environment. The lattice parameters of $SrLa_{10}Ir_4O_{24}$ are a = 11.58 Å, c = 16.24 Å, while those of $BaLa_{10}Ir_4O_{24}$ are a = 11.66 Å, c = 16.17 Å. Compared to $SrLa_{10}Ir_4O_{24}$, the Ba analogue has a larger a lattice parameter and a smaller c lattice parameter. In other words, the lattice is "squashed" rather than simply enlarged. The cell volume of $BaLa_{10}Ir_4O_{24}$ (2196.9 Å^3) is only slightly larger than that of $SrLa_{10}Ir_4O_{24}$ (2183.4 Å^3), a difference of ~0.05%. This weak volume perturbation is not surprising, because although the ionic radius of Ba^{2+} (1.42 Å) is significantly larger than that of Sr^{2+} (1.26 Å), the alkaline earth metal is only a small fraction of the unit cell contents. For $SrLa_{10}Ir_4O_{24}$, the bond length of Ir1-O ranges from 1.967(15) Å to 2.030(16) Å, while the bond length of Ir2-O ranges from 2.001(16) Å to 2.073(16) Å. For $BaLa_{10}Ir_4O_{24}$, the bond length of Ir1-O ranges from 1.983(12) Å to 2.046(12) Å, while the bond length of Ir2-O ranges from 2.006(12) Å to 2.086(13) Å. These bond lengths are typical of Ir(IV) in oxides[14,15].

The temperature-dependent magnetic susceptibility of $SrLa_{10}Ir_4O_{24}$ shows a cusp characteristic of antiferromagnetic order at T_N = 12 K (Fig. 2, top), indicating a non-negligible magnetic exchange among the isolated octahedra. Above this cusp, the magnetic behavior is well approximated as that of a Curie-Weiss paramagnet. A fit of the data to $\chi = C/(T-\theta) + \chi_0$ (where χ_0 phenomenologically accounts for all diamagnetic contributions) from 20 K to 300 K (the results are largely insensitive to the choice of fitting range) gives a Weiss constant of −8.5 K, in good agreement with T_N. The effective moment (μ_{eff}) of 1.11 μ_B/Ir is considerably reduced from the 1.73 μ_B/Ir expected for low-spin d^5 Ir(IV) in a rigorously J_{eff} = ½ configuration (cubic crystal field, $k_BT/\lambda \rightarrow 0$)[16]. We note that such reduced effective moments are not uncommonly reported among iridates, including Sr_2IrO_4 (0.50 μ_B /Ir)[17], $Sr_3Ir_2O_7$ (0.69 μ_B /Ir)[18], 9 M $BaIrO_3$ (0.13 μ_B /Ir)[17] and 6 M $BaIrO_3$ (0.276 μ_B /Ir)[19]. However, other iridates, notably Na_2IrO_3[20], with a reported μ_{eff} = 1.79 μ_B /Ir, follow more closely the expected behavior. Discrepancies such as these suggest an 'effective g-factor' significantly reduced from the free electron value, deriving potentially from non-cubic symmetry, an admixture of configurations other than t_{2g}^5, or the effect of hybridization with the O sublattice network.

Similarly, the temperature dependent magnetic measurement of $BaLa_{10}Ir_4O_{24}$ shows antiferromagnetic ordering at a somewhat lower temperature, T_N = 6 K (Fig. 2, bottom), and also follows Curie-Weiss

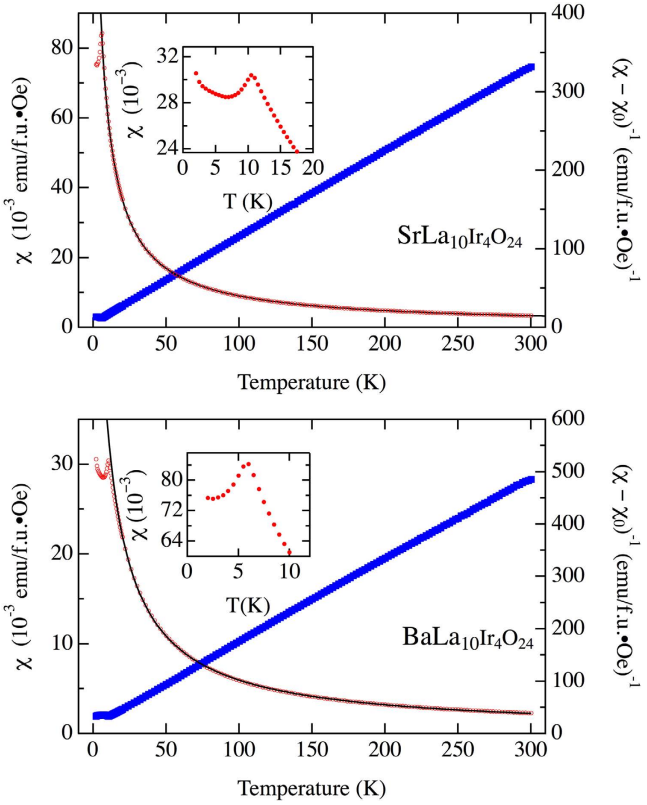

Figure 2. Temperature dependent DC magnetic susceptibility of $SrLa_{10}Ir_4O_{24}$ (top) and Ba $La_{10}Ir_4O_{24}$ (bottom). Open red circles are the data, and the solid black line is a Curie-Weiss fit including a temperature independent parameter, χ_0, which takes the values 2.2×10^{-4} emu/f.u.•Oe and 3.7×10^{-4} emu/f.u•Oe, respectively. The blue line is the inverse T-dependent component of the susceptibility. Measuring field is 5000 Oe. The insets show the low temperature ranges (**a**) $SrLa_{10}Ir_4O_{24}$ (**b**) $BaLa_{10}Ir_4O_{24}$.

behavior above this temperature, with $\mu_{eff} = 1.35\,\mu_B$, slightly larger than that of $SrLa_{10}Ir_4O_{24}$. The Weiss constant obtained is −5.1 K, close to the measured T_N. For both $SrLa_{10}Ir_4O_{24}$ and $BaLa_{10}Ir_4O_{24}$, at temperatures below the T_N, the susceptibility has a small upturn, which may arise from a small amount of paramagnetic impurity spins.

Heat capacity measurements were carried out on both compounds. Above the magnetic transition, the data can be described by the expression $C = C_{electron} + C_{phonon} = \gamma T + \beta T^3$ (Fig. 3a). The values of γ and β extracted from the fits for $SrLa_{10}Ir_4O_{24}$ are 0.405 $Jmol^{-1}K^{-2}$ and 0.00205 $Jmol^{-1}K^{-4}$, and for $BaLa_{10}Ir_4O_{24}$ γ and β value are 0.47 $Jmol^{-1}K^{-2}$ and 0.00224 $Jmol^{-1}K^{-4}$. Corresponding Debye temperatures were calculated to be 333 K for $SrLa_{10}Ir_4O_{24}$, and 324 K for $BaLa_{10}Ir_4O_{24}$. The magnetic entropy in the low-T regime can then be calculated as $S_{mag}(T) = \int_0^T C_{mag}/T\,dT$ (Fig. 3b), where $C_{mag} = C_{tot} - C_{electron} - C_{phonon}$, yielding $S_{mag} = 6.31$ J mol^{-1} K^{-1} for $SrLa_{10}Ir_4O_{24}$ and 6.17 J mol^{-1} K^{-1} for $BaLa_{10}Ir_4O_{24}$ (Fig. 3b). The expected entropy of the magnetic transition (S_{mag}) equals to $R\ln(2J+1)$, where R is the gas constant, and J is the total angular momentum. For $J_{eff} = ½$, the expected value is 5.76 J mol^{-1} K^{-1}, in fair agreement with that measured here.

Resistivity measurement shows that $SrLa_{10}Ir_4O_{24}$ exhibits insulating behavior (Fig. 4), which is expected given that the crystal structure features isolated IrO_6 octahedra. With the caveat that the behavior is evaluated in a narrow temperature range of 260 K to 350 K, it was found that the resistivity is best modeled by simple thermally activated hopping, with Ea ~0.26 eV, while three-dimensional and two-dimensional variable range hopping and small polaron models yield poorer agreement with the measured data. Unfortunately, $BaLa_{10}Ir_4O_{24}$ crystal specimens are too small for a conductivity measurement at this time. Due to the similar crystal structure, one may expect similar electronic transport behavior to that of the Sr analogue.

Discussion

Flux crystal growth is an important approach to grow single crystals of new materials[21–26]. For exploratory crystal growth of new iridates, KOH and K_2CO_3 fluxes have typically been used[27,28]. Remarkably, for the synthesis of $SrLa_{10}Ir_4O_{24}$, Ir metal was used as the source of Ir and was oxidized to Ir(IV) in the $SrCl_2$ flux. It is known that some fluxes like KOH can dissolve O_2 from the atmosphere to provide an

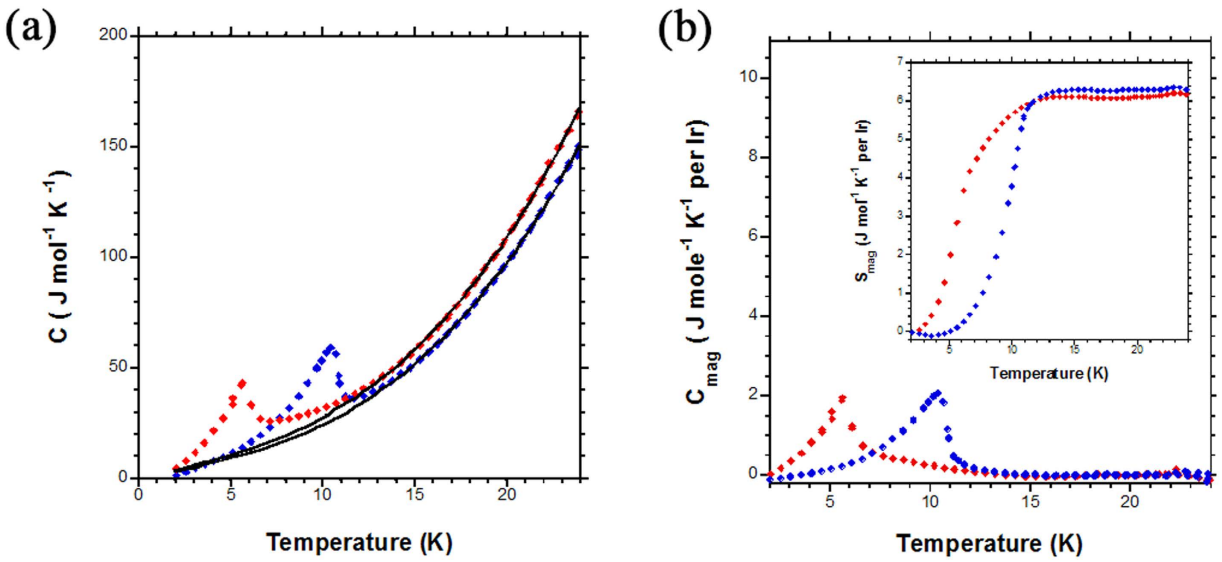

Figure 3. Heat capacity of $SrLa_{10}Ir_4O_{24}$ and $BaLa_{10}Ir_4O_{24}$. Red points are for $SrLa_{10}Ir_4O_{24}$ and blue points are for $BaLa_{10}Ir_4O_{24}$. Fits are shown in black (see text). (**a**) Total heat capacity (**b**) magnetic contribution to the heat capacity. Inset to (**b**) shows the entropy of the magnetic transition.

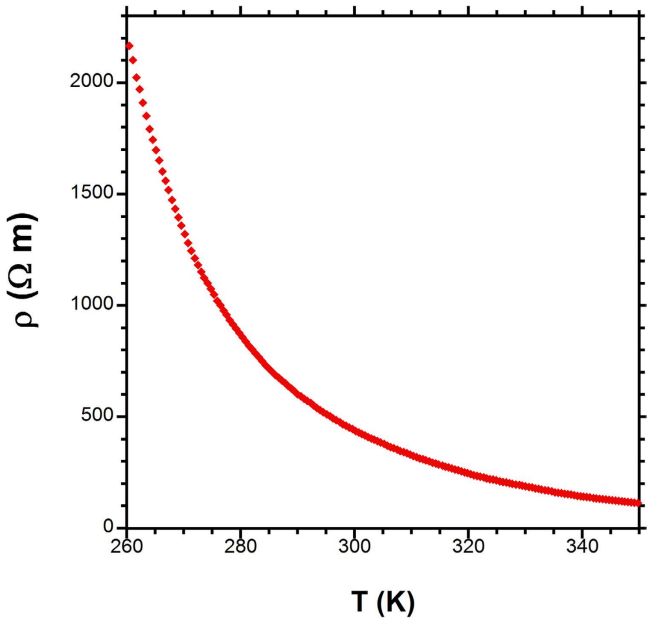

Figure 4. Resistivity vs. temperature for $SrLa_{10}Ir_4O_{24}$.

oxidizing environment; mostly Ir(V) compounds have been synthesized from KOH flux, but some Ir(VI) and Ir(V) oxides are also reported[29,30]. Evidently $SrCl_2$ also dissolves sufficient O_2 from the atmosphere to oxidize Ir metal to Ir(IV). However, under the conditions of our synthesis, $SrCl_2$ apparently provides a less oxidizing environment compared to KOH, as we found no higher oxidation state products. EDS shows no evidence of chlorine incorporation in the crystals.

$MLa_{10}Ir_4O_{24}$ (M = Sr, Ba) compounds have similar lattice parameters as the Mo(VI) oxide, $Sr_9La_2Mo_4O_{24}$[13]. Although the atomic coordinates of $Sr_9La_2Mo_4O_{24}$ were not reported[13], the stoichiometry and similar lattice parameters leads one to expect that the structures of $MLa_{10}Ir_4O_{24}$ (M = Sr, Ba) and $Sr_9La_2Mo_4O_{24}$ are closely related. Apparently this structure type can adjust its M:La ratio to accommodate either the tetravalent Ir or the hexavalent Mo. When only alkaline earth metal is involved and rare earth metal is excluded, the structure type can host transition metal with mixed oxidation states, which has been shown by the synthesis of $Ca_{11}Re_4O_{24}$[31] $Sr_{11}Re_4O_{24}$[32] and $Ba_{11}Os_4O_{24}$[33].

Magnetization data show that the effective moment of $MLa_{10}Ir_4O_{24}$ (M = Sr, Ba) is significantly reduced vis-à-vis that expected for a J = ½ Kramer's ion. In the case of 6 M-$BaIrO_3$ it has been suggested

Empirical formula	$SrLa_{10}Ir_4O_{24}$	$BaLa_{10}Ir_4O_{24}$
Formula weight	2629.52	2679.24
Temperature	293(2) K	293(2) K
Wavelength	0.71073 Å	0.71073 Å
Crystal system	Tetragonal	Tetragonal
Space group	$I4_1/a$	$I4_1/a$
Unit cell dimensions	$a = 11.5899(16)$ Å, $\alpha = 90.00°$ $b = 11.5899(16)$ Å, $\beta = 90.00°$ $c = 16.255(3)$ Å, $\gamma = 90.00°$	$a = 11.6569(6)$ Å, $\alpha = 90.00°$ $b = 11.6569(6)$ Å, $\beta = 90.00°$ $c = 16.1673(9)$ Å, $\gamma = 90.00°$
Volume	2183.4(6) $Å^3$	2196.9(2) $Å^3$
Z	4	4
Density (calculated)	7.999 g/cm^3	8.101 g/cm^3
Absorption coefficient	45.869 mm^{-1}	44.942 mm^{-1}
F(000)	4432	4504
Crystal size	$0.134 \times 0.105 \times 0.092\,mm^3$	$0.0237 \times 0.0170 \times 0.0084\,mm^3$
θ range for data collection	3.52 to 24.98°	3.53 to 29.25°
Index ranges	−13<=h<=13, −13<=k<=12, −19<=l<=19	−15<=h<=15, −15<=k<=6, −22<=l<=22
Reflections collected	6661	5180
Independent reflections	968 [$R_{int} = 0.1041$]	1424 [$R_{int} = 0.0754$]
Completeness to θ = 29.25°	99.9%	95.6%
Refinement method	Full-matrix least-squares on F^2	Full-matrix least-squares on F^2
Data / restraints / parameters	968 / 0 / 94	1424 / 0 / 93
Goodness-of-fit	1.088	1.076
Final *R* indices [>2σ(I)]	$R_{obs} = 0.0480$, $wR_{obs} = 0.1353$	$R_{obs} = 0.0532$, $wR_{obs} = 0.1219$
R indices [all data]	$R_{all} = 0.0563$, $wR_{all} = 0.1613$	$R_{all} = 0.0603$, $wR_{all} = 0.1268$
Largest diff. peak and hole	4.662 and −2.694 e·$Å^{-3}$	2.537 and −2.193 e·$Å^{-3}$

Table 1. Crystal data and structure refinement for $MLa_{10}Ir_4O_{24}$ (M = Sr, Ba) at 293(2) K.

that such a reduced effective moment may arise from the *d* electron hybridization with oxygen p states[18]. Putting any such argument on a stronger, more quantitative footing calls for a broader materials search and theoretical input beyond the scope of this report.

As mentioned earlier, the $J_{eff} = ½$ state has been implicated as foundational to the understanding of iridate physics, although this description rigorously applies only in the case of an isolated and ideal octahedral crystal field[6,7]. The former criterion eliminates band structure effects and super-exchange, while the latter guarantees the symmetry of the $J_{eff} = ½$ wavefunction (assuming that the e_g states lie at sufficiently high energy that the contribution from excited configurations such as $t_{2g}{}^4e_g{}^1$ are negligible. This latter assumption has been questioned recently by Katakuri *et al.* from quantum chemical calculations[34]. By isolating the octahedra and thus eliminating bandwidth and super-exchange as a competing influence on the electronic structure[35], compounds such as $MLa_{10}Ir_4O_{24}$ offer a platform for testing the intrinsic nature of the $J_{eff} = ½$ description.

Conclusion

In summary, we report the discovery and characterization of two new quaternary iridates, $SrLa_{10}Ir_4O_{24}$ and $BaLa_{10}Ir_4O_{24}$, with the crystal structure similar to $Ca_{11}Re_4O_{24}$[31], $Sr_{11}Re_4O_{24}$[32] and $Ba_{11}Os_4O_{24}$[33] and $Sr_9La_2Mo_4O_{24}$[13]. By isolating the octahedra and thus eliminating bandwidth and super-exchange as a competing influence on the electronic structure, compounds such as these can provide a platform for testing the detailed nature and range of applicability of the $J_{eff} = ½$ description using, for example, resonant inelastic x-ray scattering. More generally, the synthetic approaches reported here provide valuable insights that can stimulate the efforts in crystal growth of new iridates, particularly quaternary iridates, that will be essential to achieving a broader understanding of correlated electron physics in the presence of strong spin-orbit coupling.

During the proofing process of this manuscript, we became aware of a paper reporting the synthesis and magnetic properties of SrxLa11−xIr4O24 (B.F. Phelan *et al.* Phys. Rev. B 91, 155117 (2015)). The crystallographic data presented by Phelan *et al.* for single crystal Sr4.25La6.75Ir4O24 are qualitatively

Label	*x*	*y*	*z*	Occupancy	U_{eq}^{*}
$SrLa_{10}Ir_4O_{24}$					
Ir(1)	0.5000	0.5000	0	1	35(1)
Ir(2)	0	0.5000	0	1	35(1)
La(1)	0.7715(2)	0.4530(2)	0.1159(1)	1	38(1)
La(2)	0.7059(2)	0.7264(2)	0.348(1)	1	39(1)
La(3)	0.5000	0.7500	−0.1400(2)	1	52(1)
Sr(1)	0	0.7500	−0.1250	1	90(3)
O(1)	1.0087(12)	0.5358(15)	−0.1220(11)	1	44(4)
O(2)	0.8684(15)	0.6115(15)	0.0047(10)	1	46(4)
O(3)	0.3927(13)	0.4232(13)	0.0761(10)	1	44(3)
O(4)	0.5865(12)	0.5801(14)	0.0924(10)	1	42(3)
O(5)	0.6009(13)	0.3656(12)	0.0295(10)	1	40(3)
O(6)	1.1266(14)	0.6231(15)	0.0203(10)	1	42(3)
$BaLa_{10}Ir_4O_{24}$					
Ir(1)	0.5000	0.5000	0	1	16(1)
Ir(2)	0	0.5000	0	1	16(1)
La(1)	0.2307(1)	0.4543(1)	0.1156(1)	1	17(1)
La(2)	0.2942(1)	0.7263(1)	0.0341(1)	1	19(1)
La(3)	0.5000	0.7500	−0.1416(1)	1	21(1)
Ba(1)	0	0.2500	0.1250	1	22(1)
O(1)	−0.0090(11)	0.5176(11)	−0.1233(7)	1	20(2)
O(2)	0.6096(11)	0.4306(12)	0.0793(7)	1	22(3)
O(3)	0.4080(12)	0.5748(11)	0.0933(8)	1	23(3)
O(4)	0.1339(12)	0.6108(12)	0.0011(7)	1	20(2)
O(5)	0.3963(12)	0.3661(12)	0.0272(9)	1	26(3)
O(6)	−0.1304(13)	0.6204(12)	0.0165(8)	1	24(3)

Table 2. Atomic coordinates and equivalent isotropic displacement parameters ($Å^2 \times 10^3$) for $MLa_{10}Ir_4O_{24}$ (M = Sr, Ba) at 293(2) K with estimated standard deviations in parentheses. $^{*}U_{eq}$ is defined as one third of the trace of the orthogonalized U_{ij} tensor.

$SrLa_{10}Ir_4O_{24}$		$BaLa_{10}Ir_4O_{24}$	
Ir(1)-O(3)	1.967(15) × 2	Ir(1)-O(2)	1.983(12) × 2
Ir(1)-O(5)	2.006(14) × 2	Ir(1)-O(5)	2.023(13) × 2
Ir(1)-O(4)	2.030(16) × 2	Ir(1)-O(3)	2.046(12) × 2
Ir(2)-O(2)	2.001(16) × 2	Ir(2)-O(1)	2.006(12) × 2
Ir(2)-O(1)	2.028(17) × 2	Ir(2)-O(4)	2.026(13) × 2
Ir(2)-O(6)	2.073(16) × 2	Ir(2)-O(6)	2.086(13) × 2

Table 3. Selected bond lengths [Å] for $MLa_{10}Ir_4O_{24}$ (M = Sr, Ba) at 293(2) K with estimated standard deviations in parentheses.

the same as ours with a slightly smaller average Ir-O bond length that can be attributed to a slightly more Ir(V) concentration in the specimen of Phelan *et al.* Magnetic properties of the x = 1 member of this series (polycrystalline specimens in the Phelan *et al.* report) are comparable to those here, showing Curie-Weiss behavior at a cusp at ~12 K., Curiously, the effective moment for SrLa10Ir4O24 reported by Phelan et al differs considerably from that we find and is closer to that expected by an isolated Ir(IV). We do not have an explanation for this discrepancy, but note that the synthetic processes are different.

Methods

Syntheses. Crystals of the $M La_{10}Ir_4O_{24}$ (M = Sr, Ba) were grown by a flux method. For the synthesis of $SrLa_{10}Ir_4O_{24}$, La_2O_3 (Alfa Aesar, 99.9%, 0.51 mmol), Ir metal (0.5 mmol), and anhydrous $SrCl_2$ (12.6 mmol) were loaded into a platinum crucible. The crucible was placed into a box furnace, heated to 1200 °C at 300 °C/hour, held at that temperature for 12 h, cooled to 900 °C at 12 °C/hour, and finally cooled to room temperature by turning off the furnace. For the synthesis of $BaLa_{10}Ir_4O_{24}$, La_2O_3 (Alfa Aesar, 99.9%, 0.82 mmol) IrO_2 (0.82 mmol), anhydrous $BaCl_2$ (30 mmol) were loaded into a platinum crucible. The crucible was placed into a box furnace, heated to 900 °C at 300 °C/hour, then heated to 1200 °C at 12 °C/hour, held at 1200 °C for 12 h, cooled to 950 °C at 10 °C/hour, and finally cooled to room temperature by turning off the furnace. For both compounds, the crystals were separated from the flux by dissolving the flux in water aided by sonication, and then isolated with vacuum filtration and rinsing with acetone. The crystals are stable in air and water. They are black in color with an irregular polyhedral shape, and the crystal sizes are about 100 microns from one face to the face across.

Single Crystal X-ray Diffraction and EDS. Single crystals with irregular polyhedral shape were selected and mounted on tips of glass fibers for X-ray diffraction. Intensity data were collected at room temperature on a STOE imaging plate diffraction system (IPDS-II) using graphite-monochromatized Mo–Kα radiation (λ = 0.71073 Å) operating at 50 kV and 40 mA with a 34 cm diameter imaging plate. For $SrLa_{10}Ir_4O_{24}$, individual frames were collected with a 15 min exposure time and a 1° ω rotation at a φ angle of 98°, while for $BaLa_{10}Ir_4O_{24}$, individual frames were collected with a 5 min exposure time and a 1° ω rotation at a φ angle of 78°. Data reduction and integration absorption correction were performed using X-Area software provided by STOE, and the crystal structures were solved with SHELXL 97 software package[36]. The parameters for data collection and the details of the structure refinement are given in Table 1. Atomic coordinates, isotropic thermal displacement parameters (U_{eq}) and occupancies of all atoms are given in Table 2, and selected bond lengths are given in Tables 3 for both compounds. Anisotropic displacement parameters are given in the supplemental material. The isotropic thermal parameter for Sr1 in $SrLa_{10}Ir_4O_{24}$ is relatively large, and the anisotropic thermal parameters for Sr1 have an elongated ellipsoid shape. This may be a sign of disordering for this site. The Ba in $BaLa_{10}Ir_4O_{24}$, on the other hand, is well behaved. Electron dispersive X-ray spectroscopy data were collected on Oxford INCA Model 6498 and no discernible chlorine peaks were detected.

Magnetism. The DC magnetic susceptibilities of the ground samples were measured using a Quantum Design MPMS XL SQUID magnetometer. Samples were measured under zero-field-cooled (ZFC) and field-cooled (FC) conditions in an applied field of 5000 G. For $SrLa_{10}Ir_4O_{24}$, the magnetization was measured upon warming the samples from 1.8 to 300 K. For $BaLa_{10}Ir_4O_{24}$, the magnetization was measured upon warming the samples from 2 to 300 K. The very small diamagnetic contribution of the gelatin capsule had a negligible contribution to the overall magnetization and was not subtracted.

Electrical Conductivity and Heat Capacity. Electrical conductivity of a single crystal of $SrLa_{10}Ir_4O_{24}$ was measured on a Quantum Design PPMS with a four-probe method. It was found that below 260 K the resistance is too large to be measured, thus data between 260 K and 350 K were measured. Heat capacity for both compounds was measured on the PPMS from 2 K to 30 K.

References

1. Lee, P. A., Nagaosa, N. & Wen, X.-G. Doping a Mott insulator: physics of high-temperature superconductivity. *Rev. Mod. Phys.* **78,** 17–85 (2006).
2. Ramirez, A. P. Colossal magnetoresistance *J. Phys. Con. Mater.* **9,** 8171–8199 (1997).
3. Mitchell, J. F., Argyriou, D. N., Potter, C. D. & Hinks, D. G. Structural phase diagram of $La_{1-x}Sr_xMnO_{3+\delta}$: Relationship to magnetic and transport properties. *Phys. Rev. B* **54,** 6172–6183 (1996).
4. Wertheim, G. K. & Guggenheim, H. J. Conduction-electron screening in metallic oxides: IrO_2. *Phys. Rev. B* **22,** 4680–4683 (1980).
5. Qi, T. *et al.* Strong magnetic instablility in correlated metallic $Bi_2Ir_2O_7$. *J. Phys. Con. Mater.* **24,** 345601 (2012).
6. Kim, B.-J. *et al.* Novel $J_{\rm eff}$ =1/2 state induced by relativistic spin-orbital couploing in Sr_2IrO_4. *Phys. Rev. Lett.* **101,** 076402 (2008).
7. Kim, B.-J. *et al.* Phase-sensitive observation of a spin-orbital Mott state in Sr_2IrO_4. *Science* **323,** 1329–1332 (2009).
8. Kim, J. *et al.* Magnetic excitation spectra of Sr_2IrO_4 probed by resonant inelastic X-Ray scattering: establishing links to cupratre superconductors. *Phys. Rev. Lett.* **108,** 177003 (2012).
9. Wang, F. & Senthill, T. Twisted hubbard model for Sr_2IrO_4. *Phys. Rev. Lett.* **106,** 136402 (2011).
10. Wantanabe, H., Shirakawa, T. & Yunoki, S. Monte Carlo Study of an unconventional superconducting phase in iridium oxide. *Phys. Rev. Lett.* **110,** 027002 (2013).
11. Boseggia, S. *et al.* Robustness of basal-plane antiferromagnetic order and the $J_{\rm eff}$=1/2 state in single-layer iridate spin-orbit Mott insulators. *Phys. Rev. Lett.* **110,** 117201 (2013).
12. Calder, S. *et al.* $J_{\rm eff}$ =1/2 Mott spin-orbit insulating state close to the cubic limit in Ca_4IrO_6 *Phys. Rev. B* **89,** 081104(R) (2014).
13. Davydova, N. N. & Evdokimov, A. A. Phase relationships in AO-R_2O_3-MoO_3 systems. *Russ. J. Inorg. Chem.* **36,** 284–286 (1991).
14. Shimora, T., Inaguma, A., Nakamura, T., Itoh, M. & Morii, Y. Structure and magnetic properties of $Sr_{2-x}A_xIrO_4$ (A=Ca and Ba). *Phys. Rev. B* **52,** 9143–9146 (1995).
15. Schmalle, H. W., Gurtner, C., Oswald, H. R. & Reller, A. The crystal structure of $SrIrO_3$. *Z. Kristallogr.* **191,** 239–247 (1990).
16. Kotani, M. On the Magnetic Moment of Complex Ions. (I) *J. Phys. Soc. Jpn.* **4,** 293–297 (1949)
17. Cao, G., Bolivar, J., McCall, S., Crow, J. E. & Guertin, R. P. Weak ferromagnetism, metal-to-nonmetal transition, and negative differential resistivity in single-crystal Sr_2IrO_4 *Phys. Rev. B* **57,** R11039–R11042 (1998).
18. Cao, G. *et al.* Anomalous magnetic and transport behavior in the magnetic insulator $Sr_3Ir_2O_7$ *Phys. Rev. B* **66,** 214412 (2002).

19. Zhao, J. *et al.* Structural and physical properties of the 6M $BaIrO_3$: a new metallic iridate synthesized under high pressure. *Inorg. Chem.* **48,** 4290–4294 (2009).
20. Singh, Y. *et al.* Relevance of the Heisenberg-Kitaev model for the honeycomb lattice iridates A_2IrO_3. *Phys. Rev. Lett.* **108,** 127203.
21. Zhao, Q. *et al.* Intriguing interconnections among phase transition, magnetic moment, and valence disproportionation in 2H-Perovskite related oxides. *J. Am. Chem. Soc.* **133,** 20981–20994 (2011).
22. Zhao, Q. *et al.* $Ba_4KFe_3O_9$: a novel ferrite containing discrete 6-membered rings of corner-sharing FeO_4 tetrahedra. *Inorg. Chem.* **50,** 10310–10318 (2011).
23. Chance, W. M., Bugaris, D. E., Sefat, A. S. & zur Loye, H.-C. Crystal growth of new hexahydromettalates using a hydroflux. *Inorg. Chem.* **52,** 11723–11733 (2013).
24. Read, C. M., Bugaris, D. E. & zur Loye, H.-C. Single crystal growth and structural characterization of four complex uranium oxides: $CaUO_4$, β-Ca_3UO_6, $K_4CaU_3O_{12}$, and $K_4SrU_3O_{12}$. *Solid State Sci.* **17,** 40–45 (2013).
25. Han, F., Wan, X., Shen, B. & Wen, H. H. $BaFe_2Se_2O$ as an iron-based Mott insulator with antiferromagnetic order. *Phys. Rev. B* **86,** 014411(2012).
26. Zhao, Q., Bugaris, D. E., Stackhouse, C. A., Smith, M. D. & zur Loye, H.-C. Crystal growth and structure determinations of potassium hafnates: $K_2Hf_2O_5$ and $K_4Hf_5O_{12}$. *Mater. Res. Bull.* **46,** 166–169 (2011).
27. Stitzer, K. E., Smith, M. D. & zur Loye, H.-C. Crystal growth, structure determination and magnetic properties of $Ba_4Ir_3O_{10}$ and $Ba_4(Co_{0.4}Ir_{0.6})Ir_2O_{10}$. *J. Alloy & Compd.* **338,** 104–111 (2002).
28. Mugavero, S. J. III., Smith, M. D., Yoon, W.-S. & zur Loye, H.-C. $Nd_2K_2IrO_7$ and $Sm_2K_2IrO_7$: iridium(VI) oxides prepared under ambient pressure. *Angew. Chem. Int. Ed.* **48,** 215–218 (2008).
29. Lux, H. "Säuren" und "basen" im schmelzfluss: die bestimmung. der sauerstoffionen-konzentration. *Z. Elektrochem.* **45,** 303–309 (1939).
30. Flood, H. & Förland, T. The acidic and basic properties of oxides. *Acta Chem. Scand. Ser.* **B1,** 592–604 (1947).
31. Jeitschko, W., Mons, H. A., Rodewald, U. C. & Moeller, M. H. The crystal structure of the potential ferroelectric calcium rhenate(VI, VII) $Ca_{11}Re_4O_{24}$ and its relation to the structure of $Sr_{11}Os_4O_{24}$. *Z. Natur. B* **53,** 31–36 (1998).
32. Bramnik, K. G. *et al.* Preparation, structure, and magnetic studies of a new $Sr_{11}Re_4O_{24}$ double oxide. *J. Solid State Chem.* **149,** 49–55 (2000).
33. Wakeshima, M. & Hinatsu, Y. Crystal structure and magnetic ordering of novel perovskite-related barium osmate $Ba_{11}Os_4O_{24}$ *Solid State Comm.* **136,** 499–503 (2005).
34. Katukuri, V. M. *et al.* Electronic structure of low-dimensional 4d(5) oxides: interplay of ligand distortions, overall lattice anisotropy, and spin-orbit interactions. *Inorg Chem* **53,** 4833–4839 (2014).
35. Witczak-Krempa, W., Chen, G., Kim, Y. B. & Balents, L. Correlated quantum phenomena in the strong spin-orbit regime. *Annu. Rev. Conden. Ma. P.* **5,** 57–82 (2014).
36. Sheldrick, G. M. A short history of SHELX. *Acta Cryst. A.* **64,** 112–122 (2008).

Acknowledgments

The work reported here was done solely at Argonne National Laboratory and was supported by the US Department of Energy Office of Science, Basic Energy Sciences, Materials Science and Engineering Division.

Author Contributions

Q.Z. and J.F.M. designed the strategy and wrote the paper. F.H. contributed to figure 3 and figure 4, C.C.S. and H.L. contributed to table 1, J.F.M., Q.Z. and T.H. discussed and revised the manuscript.

Additional Information

Supplementary information accompanies this paper at http://www.nature.com/srep

Competing financial interests: The authors declare no competing financial interests.

How to cite this article: Zhao, Q. *et al.* New Insulating Antiferromagnetic Quaternary Iridates MLa10Ir4O24 (M = Sr, Ba). *Sci. Rep.* **5**, 11705; doi: 10.1038/srep11705 (2015).